Assimilation of sea surface salinity in a tropical oceanic general circulation model (OGCM): a twin experiment approach

Fabien Durand, Lionel Gourdeau, Thierry Delcroix, Jacques Verron

Assimilation of sea surface salinity in a tropical Oceanic General Circulation Model (OGCM): A twin experiment approach

Fabien Durand and Lionel Gourdeau
Laboratoire d'Etudes en Géophysique et Océanographie Spatiales, Toulouse, France

Thierry Delcroix
Institut de Recherche pour le Développement, Nouméa, New Caledonia, France

Jacques Verron
Laboratoire des Ecoulements Géophysiques et Industriels, Centre National de la Recherche Scientifique, Grenoble, France

[1] Observing ocean surface salinity in the global ocean is a challenging issue for future years' oceanographic activities. It is motivated by the active role of salinity that is now well recognized in ocean dynamics and ocean/atmosphere exchanges. This is particularly evident in the case of the El Nin˜o Southern Oscillation (ENSO) phenomenon in the tropical Pacific Ocean. Improvements to ocean state estimation and predictions will require that salinity observations must be taken into proper account in conjunction with temperature and altimetric data. The sensitivity of a primitive equation model of the tropical Pacific Ocean to sea surface salinity (SSS) is studied through the use of a data assimilation technique in the rather academic ''twin experiment'' context. The data assimilation technique used, the Singular Evolutive Extended Kalman (SEEK) filter, is derived from the conventional Kalman filter theory. The paper explains why such a sophisticated technique is necessary. Indeed, an empirical scheme such as the Newtonian relaxation method, used in the same conditions, fails to constrain either the observed (surface) variable or the other components of the state vector. Within the experimental context chosen, the assimilation of SSS data with the SEEK filter is able to constrain most of the model variables linked with the SSS signal. SSS information, in particular, appears relatively successful in restoring zonal velocity, which is an important variable in warm/fresh pool migration, and in simulating a barrier layer in the atmospheric convergence zones. The final analysis errors are small and stable over time. This is widely true when simulating satellite SSS observations based on the GODAE criteria (0.2 psu error, 200 km, 10 days), which shows the potential of these observations. To extend these results to a real context, the problems of model-data bias and unknown error covariances must be addressed as they are actually a strong limitation in assimilation performance when assimilating any real data set

1. Introduction

[2] Salinity has been noted as one of the fundamental fields that need to be better observed in the tropical Pacific and more adequately considered in ocean models designed to improve our understanding of and/or our ability to predict El Niño Southern Oscillation (ENSO) events [*Murtugudde and Busalacchi*, 1998; *World Climate Research Program* (*WCRP*), 1998; *Ji et al.*, 2000; *McPhaden et al.*, 2001]. This is particularly relevant for the western Pacific warm pool. There, Sea Surface Temperature (SST) can reach as high as 28–29°C, generating deep atmospheric convection and heavy precipitation, thus resulting in relatively low sea surface salinity (SSS < 35). The warm pool is also characterized by the frequent existence of a barrier layer whose thickness is given by the depth difference between the salinity-controlled density mixed layer and the deeper uniform-temperature surface layer. It has been suggested that the barrier layer plays a key role in ocean/atmosphere exchanges by inhibiting vertical mixing and trapping wind momentum

[*Lukas and Lindstom*, 1991; *Vialard and Delecluse*, 1998b; *Vialard*, 2001]. The eastern edge of the warm pool is further characterized by a well-marked zonal salinity front in the equatorial band [*Kuroda and McPhaden*, 1983; *Hénin and Grelet*, 1996; *Eldin et al.*, 1997] owing its existence to the zonal convergence of westward-moving high-salinity central Pacific waters and eastward-moving low-salinity western Pacific waters [*Picaut et al.*, 1996]. Such a front is displaced eastward during El Niño and westward during La Niña events, over distances of more than 8000 km. The barrier layer and the zonal salinity front are key related processes, as discussed in the literature (for a review, see *Picaut et al.* [2001]), and they both need to coexist in ocean models aspiring to reproduce the ocean with the correct physics. As shown by *Acero-Schwertzer et al.* [1997], ignoring the salinity effects in a model can result in unrealistic zonal currents in the warm pool. This would clearly be detrimental for ENSO prediction, considering the key role of zonal advection in ENSO mechanisms [*Picaut and Delcroix*, 1995; *Picaut et al.*, 1997].

[3] Present in situ observations of salinity in the tropical Pacific rely essentially on a Voluntary Observing Ship (VOS) program [*Hénin and Grelet*, 1996], the TAO/TRITON mooring array [*McPhaden et al.*, 1998] together with cruises servicing the array [*Johnson et al.*, 2000], occasional research cruises [*Delcroix and Eldin*, 1995], and XCTD transects [*Roemmich et al.*, 1999]. While the resulting spatial and temporal distribution of the SSS observations may be adequate in the warm pool *Delcroix and McPhaden* [2002], it is clearly inadequate for subsurface measurements on the basin scale. Satellite missions are presently being proposed to space agencies for remote sensing of SSS [*Lagerloef*, 1995; *Lagerloef and Delcroix*, 2002]. If approved, these missions will lead to combined products (satellite and in situ data) which are expected to provide high resolution, accurate SSS fields for whole basins. Moreover, recently developed methods have given promising results for estimating salinity profiles from more easily available salinity and temperature profiles [*Vossepoel et al.*, 1999; *Maes and Behringer*, 2000]. In addition, a new project (ARGO) of salinity observations in the upper 0–2000 m layer is being set up with planned deployments of about 3000 drifting buoys in the world's oceans [*Roemmich et al.*, 1999]. The potential for high quality salinity observations in future is thus good; the question remains as to how these data may be optimally combined with ocean models.

[4] Poor knowledge of the Evaporation Minus Precipitation (E-P) budget is a real drawback for models attempting to correctly simulate salinity, especially in the upper layer. Most models actually use a relaxation term toward a climatological SSS field in order to compensate for the lack of reliable E-P information. This relaxation term is clearly a makeshift solution. For example, there is no guarantee that this term, once introduced into the physical equations, will be physically consistent with the ocean interior. A possible solution may be to correct the freshwater flux in order to minimize error in the modeled SSS field [*Vialard et al.*, 2002], but this correction is not optimal. Assimilating salinity observations is also a promising way of avoiding the use of the relaxation term. Current projects in oceanic data assimilation deal mainly with sea level anomalies obtained from satellite altimeter, and with temperature profiles obtained from XBT and TAO/TRITON moorings. Data assimilation usually has a positive impact on simulations [*Chen et al.*, 1998; *Fukumori et al.*, 1999; *Gourdeau et al.*, 2000]. There are, however, some instances where assimilation appears to impair the simulations, in particular when salinity changes are not taken into account [*Ji et al.*, 2000; *Segschneider et al.*, 2000]. Very few projects assimilating salinity have been undertaken so far. For example, based on a simple Newtonian relaxation method, *Reynolds et al.* [1998] looked at the impact of observed SSS on a model performance. Their results showed that SSS information alone was not sufficient to correct the model biases in subsurface salinity.

[5] In order to make optimal use of the future combination of in situ and remotely sensed salinity measurements, the present paper addresses the impact of assimilating SSS data in an Oceanic General Circulation Model (OGCM) for the tropical Pacific. The data will be simulated and the results analyzed through twin experiments where the ''truth'' is known. This classical approach, based on Observing System Simulation Experiments (OSSEs), is justified by the use of the particular observation to be assimilated (SSS). We will address the following question: ''Are the surface-only observations sufficient for predicting subsurface properties and, if they are, how does this work?''. We will use a relatively sophisticated assimilation method which takes into account the dynamics of the system (SEEK filter [*Pham et al.*, 1998]). The sensitivity of the assimilation method will be assessed with regard to the definition of the background forecast error covariances, and we will show how a simpler method fails. We will also test the ability of future satellite SSS observations to constrain an OGCM as a function of their sampling and their accuracy. These experiments will give an idea of the pertinence of such observations in a data assimilation context. However, one must keep in mind that serious problems arise when using real data (model-data bias, unknown error covariances, etc.). These problems exceed the context of our present work, but must be addressed rapidly if we want to have confidence in any assimilation result that uses real data. Nevertheless, the OSSE approach is a necessary step before attempting assimilation of real data.

[6] The paper is organized as follows. Section 2 describes the OGCM and its ability to simulate the salinity field. Section 3 presents the reduced order extended Kalman filter used for SSS data assimilation, along with the experimental procedure and a description of the three experiments. The experiments are analyzed from a statistical point of view in section 4. The first experiment validates the model-assimilation system, the second illustrates how the ''relaxation method'' works, and the third shows results from an assimilation with the SEEK filter assimilating SSS satellite data as defined in the GODAE configuration requirement. In section 5, results from the latter experiment are analyzed from a physical point of view in order to study how the physical processes are influenced by the assimilation. The final section draws our conclusions.

2. The Model and Its Salinity Field

2.1. The Model

[7] The model used is the OPA OGCM originally developed at the Laboratoire d'Océanographie Dynamique et de Climatologie (LODYC) in Paris, France [*Madec et al.*, 1998]. It is based on primitive equations, and it uses a z-coordinate on the vertical axis. The present version, named ORCA, is a free-surface version which ensures ocean salt conservation [*Roullet and Madec*, 2000]. The vertical eddy coefficients are computed from a 1.5 turbulent closure model in which the evolution of the turbulent kinetic energy is given by a prognostic equation [*Blanke and Delecluse*, 1993]. The temporal scheme is a leapfrog scheme with an Asselin filter, with the exception of vertical diffusion calculations (which use an implicit scheme) and horizontal diffusion calculations (which use a forward scheme).

[8] The model domain is global. It has a 2° zonal resolution and a variable meridional resolution varying from 0.5° at the equator to 2° poleward of 20° in latitude. The model has 31 vertical levels, and the vertical resolution varies from 10 m in the first 120 m to 500 m at the bottom. A time step of 5760 s (1.6 h) was used. A coupling between the ocean surface heat fluxes and SST is approximated by a local restoring term to observed SST [*Vialard et al.*, 2001] in order to avoid unrealistic climatic drift. Despite our poor knowledge of fresh water fluxes, the modeled SSS is not restored to climatology salinity, as is the custom, so as to study the behavior of SSS data assimilation. The model has been used extensively for process studies and validated against in situ observations in the tropical Pacific Ocean. For example, *Vialard and Delecluse* [1998a, 1998b] used this model in their study of barrier layer formation mechanisms in the western equatorial Pacific.

[9] In all our simulations, the forcing fields come from the European Center of Medium range Weather Forecasting (ECMWF). Monthly climatology for wind stress and daily climatology for the net heat and freshwater budgets are used. Interannual forcing will not be considered in the present paper as, in this context of twin experiments, the analysis pertaining to SSS assimilation is not dependent on the forcing used. The SST is relaxed to the *Levitus et al.* [1994] observed climatology monthly cycle. Starting from rest, with the Levitus salinity and temperature data, the model is spun up for 5 years; only the last year (sampled every 9 days) is analyzed.

2.2. The Simulated Salinity Field

[10] This section focuses on the free model simulations of the salinity field with reference to the observations. The mean and seasonal variations in SSS are analyzed first, then the subsurface salinity, and finally the barrier layer structure. Greatest attention should be devoted to regions where maximum salinity variability is observed and where the SSS assimilation will be particularly sensitive.

2.2.1. Sea Surface Salinity

[11] The spatial distribution of the mean simulated SSS is shown in Figure 1a. In qualitative agreement with observations [*Levitus*, 1986; *Delcroix*, 1998], the simulated SSS portrays low salinity waters (SSS < 35) below the average position of the ITCZ (Inter Tropical Convergence Zone) and SPCZ (South Pacific Convergence Zone), and also in the warm pool area—also defined as the fresh pool [*Hénin et al.*, 1998]. Also qualitatively consistent with observed SSS, high-salinity is predicted in the vicinity of French Polynesia and north-west of the Hawaiian islands (the latter is not visible in Figure 1a which only extends to 20°N). These features almost mirror the mean E-P distribution [*Delcroix et al.*, 1996]. It is interesting to note that the position of the 35 isohaline separating the salty surface waters from the fresher waters is generally consistent with the observations, except in the SPCZ where it extends too far to the south-east. This 35 isohaline has been used to delineate the eastern edge of the warm pool [*Delcroix and Picaut*, 1998].

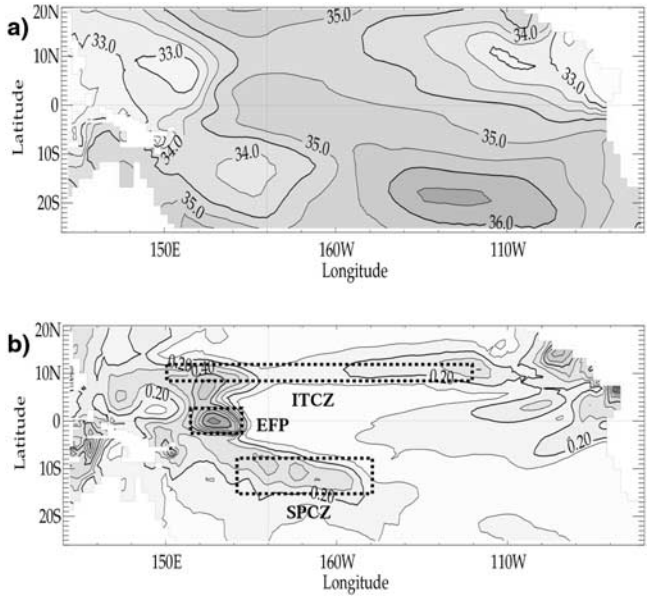

Figure 1. a) Mean SSS from the climatological run. Iso-contours are every 0.5 psu. b) Standard deviation of SSS from the climatological run. Iso-contours are every 0.1 psu. EFP, ITCZ, and SPCZ areas are defined by dotted lines.

[12] A quantitative comparison with observed features indicates that the modeled values are too fresh in the ITCZ, the SPCZ and the warm pool area. The fresh bias is typically around 0.5 and can get as high as 2, north of Papua-New Guinea. Although the model was initialized with the *Levitus et al.* [1994] data, the SSS bias appeared rapidly during the early stages of the model run, to reach a quasi-steady state after about 4 years. We believe that this SSS bias chiefly reflects the unrealistic E-P field we used. For perspective, the mean ECMWF E-P field is about twice as strong (in absolute values) as the corresponding field from the National Centers for Environmental Prediction (NCEP) in the ITCZ, SPCZ and in the warm pool.

[13] The standard deviation of the simulated SSS over the final year of simulation is shown in Figure 1b. Maximum variability (>0.25) occurs in the convergence zones, in the eastern equatorial Pacific and at the Eastern edge of the Fresh Pool (EFP). An EOF analysis (not shown here) indicates that changes under the ITCZ and SPCZ are strongly annual, with maximum SSS in March/April in the ITCZ, and in September/October in the SPCZ. These annual changes, consistent with observed features [*Delcroix*, 1998], result mainly from annual changes in the

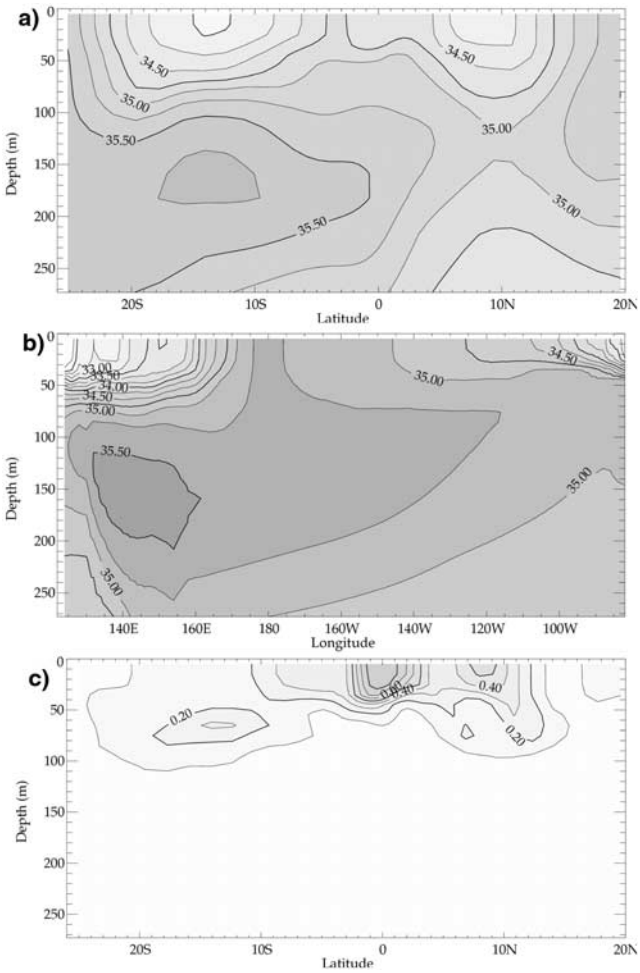

Figure 2. a) Mean latitude–depth section at 165°E, and b) mean longitude–depth section along the equator of modeled salinity. Iso-contours are every 0.25 psu. c) Standard deviation of modeled salinity along the latitude–depth section at 165°E. Iso-contours are every 0.1 psu.

E-P field. A comparison with the SST field indicates the SSS changes in the eastern equatorial Pacific result chiefly from variability in the equatorial upwelling, with maximum SSS in September at the time of minimum SST. Finally, maximum SSS variability in the region of 0°–165°E is linked to the seasonal zonal migration of the zonal salinity front located slightly west of the mean 35 isohaline (Figure 1a).

2.2.2. Subsurface Salinity

[14] The latitude–depth distribution of the mean and RMS modeled salinity along 165°E, together with the longitude–depth distribution along the equator are shown in Figure 2. Along 165°E longitude, there is significant asymmetry between the salinity structures of the northern and southern hemispheres. The southern tropical Pacific exhibits a subsurface salinity maximum [*Donguy*, 1994]. This maximum is clearly visible at depths of 150–200 m, extending from the southern tropical basin to the equatorial region (Figure 2a). This high salinity water in the middle of the thermocline is denoted as Tropical Water [*Kessler*, 1999]. This Tropical Water originates from the French Polynesian area. Salty surface water is subducted while travelling westward and toward the equator. Reaching the equator in the western basin, this water mass is then advected eastward by the Equatorial Under Current (EUC). The salinity maximum extends along the equator, from 150 m depth in the West to around 100 m in the East (Figure 2b). Along this path, the maximum salinities decrease from 35.6 in the West to 35.0 in the East. This description is in line with the *Levitus* [1994] climatology as well as the study conducted by *Donguy* [1994].

[15] In the equatorial band (Figure 2b), a well-marked zonal salinity gradient centered at 170°E appears, reaching from the surface down to about 60 m depth. Salinity values less than 34.5 (a possible proxy for the halocline) are found west of this longitude in the upper 60 m. The eastern edge of the equatorial basin also exhibits marked haline stratification with values ranging from 33 at the surface to 35 at 50 m depth, in accordance with previous studies [*Donguy*, 1994]. The low SSS in the convergence zones and in the warm pool can be traced down to about 50–80 m depth (Figure 2a).

[16] Salinity variability is mainly confined to the top 100 m at 165°E longitude (Figure 2c), with maximum variability trapped at the equator in the upper 50 m, consistent with observations [*Delcroix and Picaut*, 1998]. At greater depths, two patches of relative maxima are seen centered near 12°N and 12°S at 70 m depth, in relation with the mean position of ITCZ and SPCZ. This subsurface variability is a seasonal signal in opposite phase with the seasonal surface variability (not shown). It reflects the migration of salinity and temperature structures by vertical advection associated with the seasonal cycle of Ekman pumping [*Kessler*, 1990]. In the eastern equatorial Pacific, the mean thermocline is shallow and salinity variability there is concentrated in the upper 50 m, north of 5°S (Figure 1b). There are various possible causes for this variability. Part of it may be due to evaporation and precipitation balances affected by the displacements of the ITCZ, while part may be due to the fluctuations of zonal current in the eastern Pacific, just north of the equator. Surfacing of relatively salty equatorial undercurrent water also contributes to salinity variability in this region [*Lukas*, 1986].

2.2.3. Barrier Layer Structure

[17] As discussed in the introduction, the barrier layer is a robust climatology feature of the tropical Pacific and as such should appear in model outputs. The simulated barrier layer is indeed present in our model run, and is in relative agreement with the observed barrier layer (Figure 3a). The mean thickness of the modeled barrier layer (computed as in the work of *Vialard and Delecluse* [1998a] using the *Sprintall and Tomczak* [1992] criterion) is about 15 m in most parts of the western basin (Figure 3a). The variability signal centered at [22°S, 110°W] (Figure 3b) is an artifact of the barrier layer computation because no barrier layer exists inside this area (see Figure 3a), i.e. the barrier layer thickness computed is negative. Maximum variability in the barrier layer thickness (Figure 3b) is observed near the eastern edge of the warm pool extending to the Central basin, near the mean location of ITCZ, and in the southwestern part of the basin. These features are consistent with the analysis of interannual changes performed by *Vialard and Delecluse* [1998b]: in the equatorial region, west of the date-line, a barrier layer is formed west of the zonal salinity

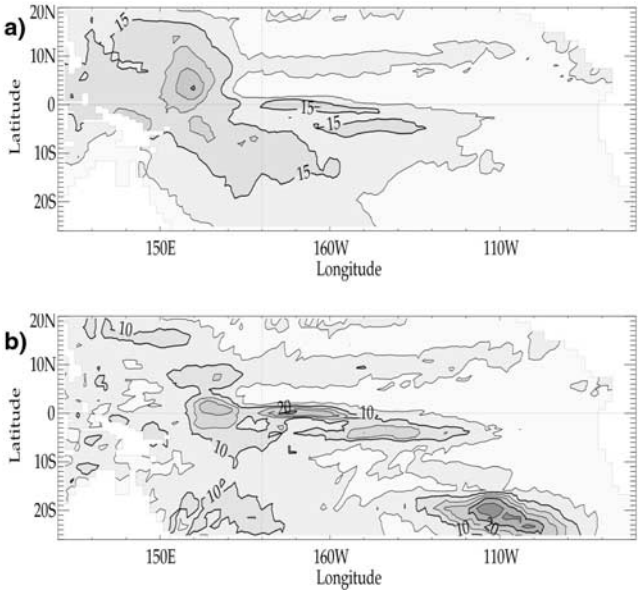

Figure 3. a) Mean, and b) standard deviation of the modeled barrier layer thickness computed using *Sprintall and Tomczak* [1992] criterion. Iso-contours are every 10, and 5 m for (a), (b) respectively.

front and follows the zonal oscillations of the front; below the ITCZ, the simulated barrier layer thickens with the seasonal increase of freshwater supply, and vice versa.

[18] The model has been validated by analyzing its salinity signature. The distribution and variability of surface and subsurface salinity fields are relatively close to the observed structures. Nevertheless, a bias in salinity may exist in the model compared to the climatology signal, because there is no relaxation to a climatological SSS field in this model run. It is not a problem in the twin experiment context developed here, which focuses on SSS variability. The variability is mainly concentrated in specific areas like the convergence zones and the warm pool that exhibit a signature in terms of barrier layer. These areas are thought to play a significant role in assimilating SSS data.

3. Assimilation Method and Experiments Description

3.1. The Seek Filter

[19] The assimilation method we used is sequential and derived from the conventional Kalman filter (KF). In essence, the Kalman filter consists of performing sequential corrections to the model trajectory by optimally weighting the accuracy of the model predictions and of the observed quantities. The Kalman filter provides the best linear unbiased estimation of the system state if the model dynamics are linear and if the statistics of the observation and model errors are perfectly known and uncorrelated. In practice, observation and overall model errors are not known. Even more importantly, the Kalman filter cannot actually be implemented in most real-life situations because of the excessive number of computations and the size of the matrices involved. This is basically due to the enormous size of the state vector in geophysical systems. A variety of methods have been proposed in the literature to reduce the computational burden of the Kalman filter and to make it tractable in the framework of oceanographic problems in particular. Some approaches [e.g., *Fukumori and Malanotte-Rizzoli*, 1995; *Cane et al.*, 1996] used the concept of reduced order space to define the prediction error covariance matrix which is the most computationally expensive part of the algorithm, especially its propagation in time.

[20] The SEEK filter, introduced by *Pham et al.* [1998], is also based on this concept. The basic assumption of the SEEK filter consists of taking an initial forecast error covariance matrix (P_0) of reduced rank and assuming that this rank is preserved in time. The rest of the KF algorithm is kept unchanged. In principle, the error covariance matrices can be projected onto the reduced basis in various ways. In our case, P_0 is initially represented by a limited number of three-dimensional, multivariate EOFs, describing the dominant modes (L) of the system's variability, and it is thus expressed as LL^T. Therefore the error corrections are made in the direction where they are naturally amplified. The 3-D multivariate approach will further allow information from the observed quantities to be spread to the whole state vector through the KF algorithm. The SEEK filter has been designed for a large variety of basin-scale ocean models and measurement types. In particular, it has been tested and validated in the tropical Pacific Ocean [*Verron et al.*, 1999; *Gourdeau et al.*, 2000].

[21] We applied the data assimilation only in the region of interest, i.e. the tropical Pacific, even though the model works on global scale. The tropical Pacific domain is defined between 20°N and 25°S latitude and from the American coast to 120°E longitude (including the Indonesian throughflow). The latitudinal asymmetry enables better integration of the signal in the SPCZ. An EOF analysis, used to define the reduced basis, is performed on the area of interest extending to, and including, a buffer zone. The buffer zone is used to connect the tropical Pacific domain to the rest of the ocean. Taking into account the decorrelation scale, the buffer has a 10° latitudinal extension along the north and south boundaries with a 30° zonal extension along the western boundary. In the buffer zone, all fields are relaxed to their mean; by doing this, the variability signal represented by the EOF modes decreases to zero along the boundaries of the extended domain.

[22] The model error covariance matrix is crudely defined as a fraction of the forecast error covariance matrix by amplifying the weights associated with the basis vectors in the reduced space with a "forgetting vector" [*Pham et al.*, 1998]. In the case of twin experiments, the definition of such model errors has little relevance because both data and model represent the same physics. This would not be the case in real-life situations in which more attention would need to be paid to this difficult aspect of the assimilation problem. Although a standard leapfrog temporal scheme is used when the model evolves between two time steps, it cannot be used after an assimilation stage. Indeed the leapfrog scheme needs two model states, whereas assimilation corrects only one state vector. Therefore, an Euler scheme is used to restart the model after each assimilation stage. Some additional operations are necessary in order to restart the

model properly, in particular to reinitialize the turbulent vertical mixing coefficients.

3.2. Experiments Description

[23] The twin experiments approach is used, in which simulated data are assimilated into the numerical model while a benchmark experiment (REF) provides the necessary data set for reference and validation. The experiments consist of recovering the true model trajectory from a simulation evolving with an erroneous initial condition, by assimilating SSS data. The assimilation is expected to be able to correct the improper trajectory of the model that would result from this ''wrong'' initial condition.

[24] The reduced basis, on which the error covariance matrices are projected, is deduced from a Multivariate EOF (MEOF) analysis of the reference fields (REF) sampled every 9 days over the last 1-year period of the free model run. Therefore, the complete basis is defined by 40 MEOFs. The first 5 vectors account for 90% of the variance of the SSS signal. The initial condition, for an academic assimilation experiment, would theoretically be the average state vector computed over the period considered for the EOF analysis, since it is the centered state of the variability analysis [see *Pham et al.*, 1998]. This average condition is chosen as initial condition to illustrate the statistical behavior of the assimilation (section 4). Also, to illustrate more clearly some physical impacts of the assimilation, a specific instantaneous field is sometimes chosen as an erroneous initial condition (section 5). The simulated data are extracted from the reference run (REF). Observations of SSS have been defined either on every model grid point of the assimilation area, or on an appropriate subgrid mimicking a typical satellite sampling (designed according to the GODAE requirement). The observations are assimilated every 9 days, and can be artificially contaminated by specific noise. The observation error covariance matrix is defined from this artificially added noise. A three-month period was found long enough to assess the assimilation experiments; therefore, all the experiments described below are conducted over this short period, and the initial stage is chosen to be the first of January, except for one experiment (see section 5).

[25] Three experiments are presented:

-*Validation experiment* (*ASS-1*) This simple experiment validates the implementation of the SEEK filter: the reduced basis is complete (all the modes are retained), and the observations are perfect. In this case, the assimilation is expected to converge to the reference.

-*SSS relaxation experiment* (*ASS-2*) The experiment ASS-2 illustrates the limitation of a too simple assimilation method. The SEEK filter was downgraded by using only the SSS univariate EOF modes in the reduced basis, suppressing the covariances between SSS and the other model variables. In this way, the assimilation works as a simple Newtonian relaxation. *Reynolds et al.* [1998] assimilated real SSS data using such a method and reported no impact of SSS data on the subsurface fields, but it is not clear if their results suffer from the method or from the fact that they use real observations.

-*SEEK/SSS GODAE experiment* (*ASS-3*) The experiment ASS-3 presents the results which may be expected from a SSS satellite data assimilation where the data are defined according to the proposed GODAE accuracy requirement. Currently, GODAE accuracy requirement is specified for large scale studies: uncertainty of $0.1-0.2$ psu over a 10-day period at $2^\circ \times 2^\circ$ resolution. Preliminary estimates suggest that this resolution can be theoretically attained from satellite measurements assuming uncorrelated and unbiased errors, and a large number of bin-averaged samples [*Lagerloef and Delcroix*, 2001]. In reality, a host of large geophysical and sensor calibration errors are not taken into account, and indeed cannot be precisely assessed yet. Satellite SSS observations have been simulated from the SSS reference fields smoothed, and sampled according to the GODAE spatial sampling scale. At this stage, the number of observations is around 1800 (versus 3100 in the previous experiments). The error introduced by this sampling procedure is around 0.06 psu RMS over the whole basin, and reaches 0.1 psu RMS in the EFP area. This error level is much smaller than that estimated by *Lagerloef and Delcroix* [2001] with real observations, because of the characteristics of the initial grid. Considering an instrument noise of 0.2 psu, the observation error (supposed to take into account both instrumental and sampling errors) is defined by a noise with RMS of 0.2 psu. The reduced basis is truncated to take into account only the most dominant SSS modes. We retained 5 modes which explain 90% of the SSS variability.

[26] The experiments take between 4 and 12 hours of CPU time of a CRAY-SV1 computer for a 3-month experiment depending on the dimension of the reduced basis. The assimilation performance depends on a number of parameters, such as the truncation of the basis, instrumental noise, error due to missing physics not represented by the assimilation system, and the number of observations assimilated. Results are discussed in the two next sections.

4. SSS Assimilation: Statistical Results

[27] Statistical analyses of the assimilation (ASS) convergence toward the reference run (REF) are made, in comparison with the model trajectory (MOD) evolving freely from its erroneous initial condition. Results of the various experiments are analyzed by regarding at the time evolution of the error (Rms Difference or RMSD between ASS-X and REF) as a percentage of the free model error (RMSD between MOD and REF) for the various variables of interest and various depths at the same instant. The variables chosen are temperature, salinity and zonal velocity, and the three depths selected represent the surface ($z = 0$ m), the mixed layer depth (around 60 m), and a deeper surface characterized as the level of maximum subsurface variability (around $100-150$ m). RMSDs are computed over the whole basin. Assimilation will impact positively (negatively) if the ratio (RMSD (ASS-REF)/RMSD (MOD-REF)) is less than (greater than) to 1. These error percentages take into account both the assimilation error reduction and the free model evolution (shown in Figure 4). But first we consider the behavior of the free model (MOD) prior to analyzing the assimilation results.

4.1. Model Without Assimilation

[28] The time evolution of the model without assimilation (MOD) is compared to that of the reference run (REF) by considering the different model variables at the surface and subsurface (Figure 4). With regard to salinity, the

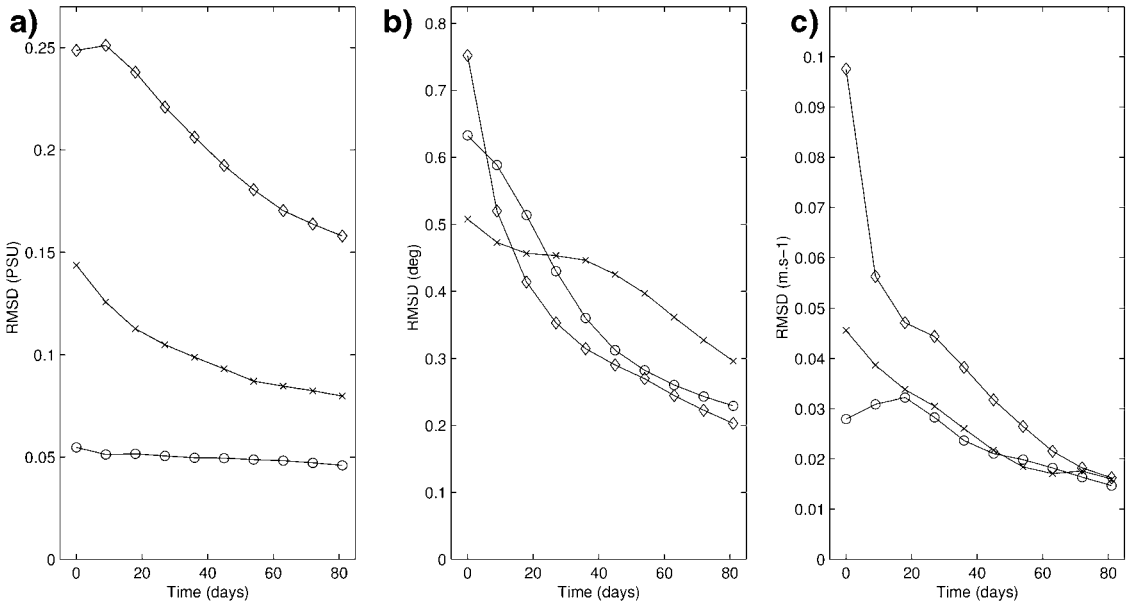

Figure 4. A 3-month evolution of the model without assimilation, initialized with the mean model state for (a) the salinity field, (b) the temperature field, and (c) the zonal velocity is plotted by comparison with the reference run (RMSD MOD-REF). Three depths are selected: the surface (diamonds), the mean mixed layer depth (60 m, x), and below (o) in the halocline (100 m) for salinity or in the thermocline (150 m) for temperature and zonal velocity.

greatest errors are concentrated in the upper 50 m, representative of the mixed layer (Figure 4a). The initial error decreases with depth from 0.25 psu at the surface to 0.05 psu at 100 m depth. After the 3-month run, the errors have decreased to 20%–45% of the initial errors: the final error varying from 0.16 psu at the surface to 0.04 psu at 100 m depth. Temperature exhibits rather different behavior (Figure 4b). As expected, the initial errors are considerable at the thermocline level (120–150 m depth), more than 0.6°C. Above the thermocline, the initial errors are smaller except near the surface (upper 30 m) where they reach 0.7°C. This can be explained by the strong influence of the surface forcing fluxes at these levels. With time, the errors decrease to 40%–73% of the initial errors. SST error decreases quickly to a low level of 0.2°C, which is the effect of the SST relaxation to climatology values. At the thermocline level, the final error falls to a similar low level (0.23°C). The error reduction is less at levels above the thermocline with final errors in the 0.3–0.4 °C range. As for zonal velocity (Figure 4c), the initial errors decrease with depth from 0.1 m/s at the surface to 0.03 m/s at thermocline level. The natural evolution of the free model shows fairly quick convergence at the surface. After the 3-month run, the errors have decreased to 50%–85% of the initial errors, and converge to the same 0.016 m/s final error.

[29] In conclusion, the freely evolving model converges slowly toward the reference, but three months is too short a period for the model to forget the initial condition and to recover its true state.

4.2. Model With Assimilation

[30] Results for the three experiments ASS-1, ASS-2, and ASS-3 presented in section 3.2, are described separately since their objectives are different. For every experiment, the time evolution of the percentage of error reduction for the different variables are plotted together in Figure 5.

4.2.1. Validation Experiment

[31] The first assimilation experiment (ASS-1) is the validation experiment of the assimilation algorithm. Here we consider perfect SSS observations on the model grid and a reduced basis which is complete in the sense that all the vectors resulting from the MEOF analysis are retained. In this academic experiment, where the initial condition is in complete accordance with the error covariance matrix P_0 computed from the reduced basis, the information provided by the SSS data must be sufficient to constrain the variables of the whole system. The SEEK filter works perfectly, since all the model variables converge rapidly to the reference after the first assimilation time stage (Figure 5, dash-dotted lines). Beyond this first time stage, the assimilation run remains close to the reference run, apart from some residual inaccuracy due to the Euler scheme associated with restarting of the model at every assimilation time stage (see section 3.1). This result validates the model/assimilation system used.

4.2.2. SSS Relaxation Experiment

[32] During the first assimilation time stage, the SSS field evolves in experiment ASS-2 as in experiment ASS-1 (Figure 5a). This is not surprising, as the reduced bases used in the ASS-1 and ASS-2 experiments show similar signals in SSS. In contrast to the multivariate analysis of ASS-1, the covariances between SSS and the other model variables are null in experiment ASS-2, and therefore the SSS information propagates as an intrinsic model adjustment. In practice, this downward propagation is achieved mostly through vertical mixing. The surface constraint on the subsurface is not immediate, and there is retroaction from the subsurface to the surface. Therefore, SSS is constrained by both the

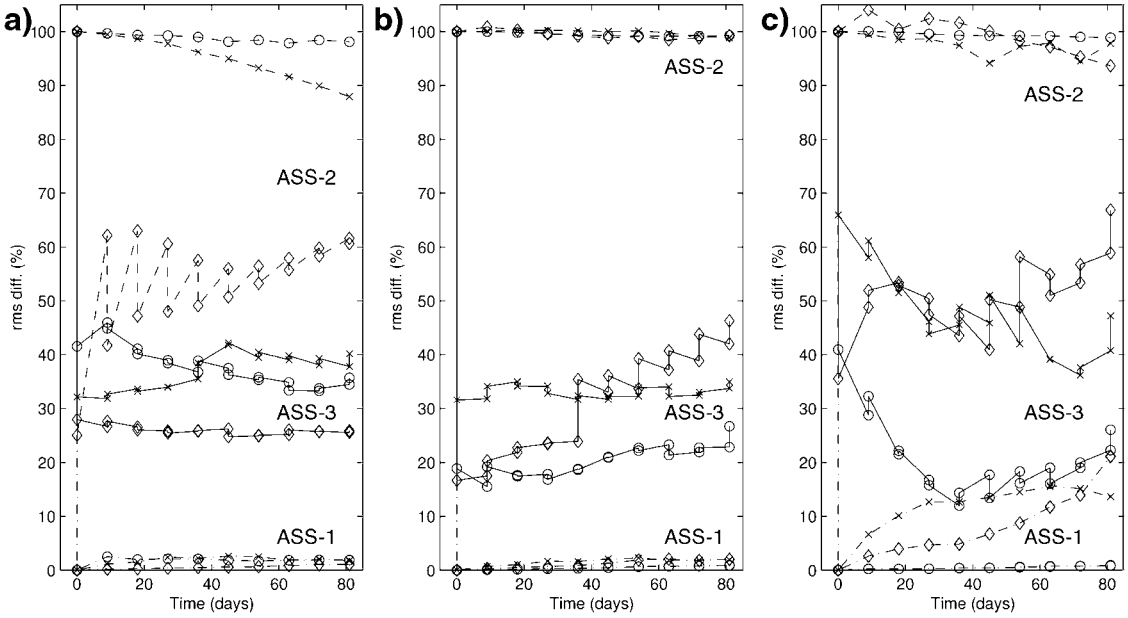

Figure 5. Impact of SSS assimilation on the a) salinity, b) temperature, and c) zonal velocity fields. Results from the three assimilation experiments are presented: ASS-1 (dash-dotted line), ASS-2 (dashed line), and ASS-3 (continuous lines). The same three depths as in Figure 4 are selected. The time evolution of the error RMSD (ASS-REF) is defined as a percentage of the free model error RMSD (MOD-REF). Both the prediction and the analysis stages are plotted.

assimilation and the subsurface which has its own memory of its previous trajectory. As expected, the SSS cannot converge to the reference as well as in the case of ASS-1. At the end of the assimilation period, the error level on salinity is about 0.1 psu at the surface, which is only a 40% error reduction. In the mixed layer, error reduction is only 12% (0.07 psu error), and at the mean halocline depth (100 m), there is no influence of surface information. This experiment is unable to constrain the model temperature, either at the surface or subsurface (Figure 5b). It has almost no effect on the velocity field (Figure 5c), except for a slight decrease in the surface error which illustrates the influence of SSS on the horizontal pressure gradients.

[33] In conclusion, a relaxation method such as the downgraded version of the SEEK filter used here, is not satisfactory. It is unable to effectively control the subsurface ocean. In addition, surface control is impaired because of the retroaction of the subsurface layers.

4.2.3. SEEK/SSS GODAE Experiment

[34] The experiment ASS-3 illustrates the performance of the SEEK filter when applied in more realistic conditions. In this case the observations are distributed according to the proposed GODAE resolution requirement for satellite sampling with a typical observation error of 0.2 psu rms. The initial forecast error covariance matrix is estimated from a truncated reduced basis for which only the dominant SSS modes are retained. Nevertheless, this experiment is far from a real-word application as the error covariance matrices for both the observations and the forecast are perfectly known. The assimilation performance is sensitive to the truncating level of the basis, the instrumental noise, and the data sampling. We discuss first the effects of each individual error source.

[35] The error introduced by the data subsampling procedure is relatively low, around 0.06 psu RMS over the whole basin (e.g., section 3.2), because of the rather coarse resolution of the initial grid. The ability of SEEK to filter noisy data is tested by adding white noise to the SSS observations, in accordance with the definition of the observation error covariance matrix. Various error levels are tested. The assimilation successfully filters the noise because we have a perfect knowledge of the error statistics. We have chosen an error of 0.2 psu Rms (signal-to-noise ratio of 1) for this experiment, and the residual error in SSS is constant in time at around 0.02 psu Rms. This residual SSS error introduces an error of around 10% of the variance of every variable (0.05°C Rms error for T at 60 m, for example). Considering a strong error of 2 psu Rms, the residual error in SSS is 0.08 psu Rms, and for the other variables it is around 35% of their variance (0.3°C for T at 60 m). So far, the complete reduced basis (40 MEOFs) has been considered. This is a large number of modes, and not all may be relevant to the SSS signal. 5 modes are enough to account for nearly all the SSS signal variance (90%) and to converge to an error level of less than 0.1 psu. The very few number of MEOFs used here is conditioned by the climatological SSS cycle, more MEOFs will be relevant when considering inter annual variability. More severe truncating can lead to relatively large errors. The sensitivity of the SSS data assimilation to the basis, as shown by twin experiments, could be a strong limitation in a real-life context.

[36] Hereafter, the cumulated effects of these errors are analyzed for the different variables in terms of relative and absolute Rms error (Figure 5 and Figure 6, respectively). For salinity (Figures 5a and 6), at the initial stage, there is a 73% error reduction at the surface corresponding to a 0.07

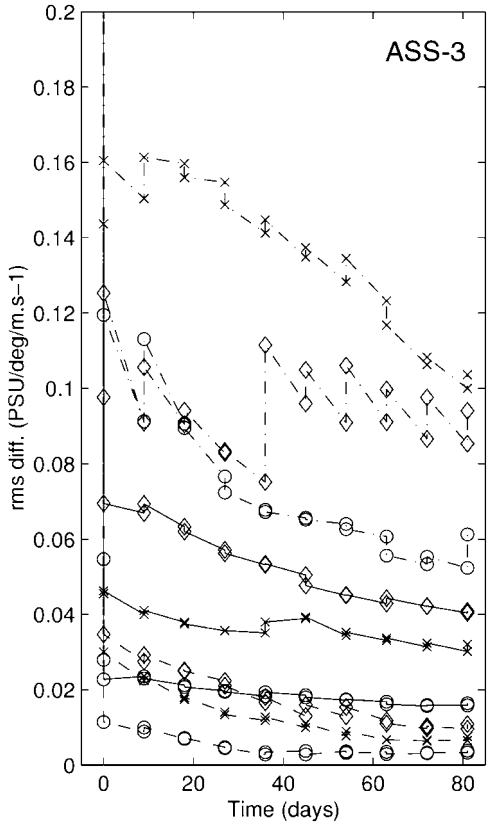

Figure 6. Time evolution of the RMSD (ASS-REF) for salinity (continuous line), temperature (dash-dotted line), and zonal velocity (dashed line) at the three depths: 0 m (diamonds), 60 m (x), 100–150 m (o). Units are psu, °C, and m/s for salinity, temperature and zonal velocity respectively.

psu Rms error. At the mixed layer depth, salinity is relatively well constrained by the SSS observations with a 68% error reduction corresponding to a 0.045 psu Rms error. In the halocline, below the mixed layer depth, the truncated basis is slightly less efficient and propagates information with a 59% error reduction, corresponding to a 0.025 psu Rms error. At the final stage, these residual errors are roughly halved due to the model propagation. For surface temperature (Figures 5b and 6), assimilation performs well with a 83% error reduction at the initial stage. With time, assimilation becomes inefficient but SST is largely conditioned by the relaxation of the model toward climatological values, limiting the impact of the assimilation. The residual error decreases for the 3-month period from 0.16°C Rms to 0.1°C Rms. The temperature control is better in the thermocline than in the mixed layer with an 81% and 68% error reduction respectively. In the mixed layer, the residual error remains relatively constant in time with a 0.12°C Rms. In the thermocline, characterized by the strongest temperature variability, the residual error decreases markedly with time from 0.12°C Rms to 0.06°C Rms. For zonal velocity (Figures 5c and 6), at the initial stage, results are poorer in the mixed layer either the surface or the deepest layers with only a 32% error reduction against a 64% and 59% error reduction, respectively. The residual errors decrease with depth from 0.03 m/s Rms to 0.01 m/s Rms, and they diminish with time even if the error reduction is only 32% at the final stage for the surface velocity. SSS assimilation appears less effective in controlling zonal velocity than temperature or salinity. The zonal velocity has a smaller order of magnitude than other variables, so velocity variability is spread over more MEOFs than are used here, which limits the efficiency of the assimilation.

[37] To conclude this section, the potential of the full SEEK filter is clearly apparent, as the multivariate approach allows significant control of the whole model state vector. Most of the information provided by the assimilation is effective at the first assimilation time stage. This idealized SSS satellite assimilation experiment gives an error reduction between 30% and 80% depending on the model variables. The SSS data assimilation is relatively efficient in influencing the salinity within the mixed layer, and the temperature within the thermocline. The error levels remain weak with regard to the signal considered (between 5% and 15% of their variance), although larger errors can occur locally (up to 0.2 psu in SSS in the EFP area and up to 0.3°C in temperature in the eastern part of the basin). At this stage, we recall that these academic experiments have limitations for real-life applications, but they are a necessary first stage of investigations.

5. Physical Impact of SSS Assimilation

[38] The impact of SSS data assimilation is analyzed from a physical point of view in some areas where salinity plays a significant role: the EFP, ITCZ, and SPCZ areas (Figure 1b), notably by the existence of a barrier layer. In order to do so, it appeared that the mean fields used as initial conditions were not relevant for such an analysis. For example, it is meaningless to compute a barrier layer thickness using those mean fields, which are too smooth. Hence, we chose an instantaneous field as initial condition, taking advantage of the contrast between two extreme situations to build our assimilation experiment. As before, we considered a 3-month period for the assimilation sequence.

[39] The EFP area delimits the region over which the zonal salinity front migrates. West of the salinity front, the fresh surface water is mostly affected by entrainment and surface forcing. Most of the literature about the eastern fresh pool's dynamics refers to inter-annual events, but it seems that most of these results are also valid at annual timescale in our climatological experiment (Figure 7). The salinity front delineates the separation between an area with near-zero SST gradient in the warm pool and a well-defined negative and nearly uniform zonal SST gradient further east [*Picaut et al.*, 2001]. This frontal zone is a permanent feature in the model results. The simulated SSS gradient in the frontal zone is around 0.2 psu per degree of longitude, in good accordance with the scarce observations [*Eldin et al.*, 1997; *Hénin et al.*, 1998]. It evidences the existence of an oceanic zone of convergence at the eastern edge of the Warm Pool. This convergence is due to the mean zonal currents in the equatorial band that are weakly eastward in the warm pool and clearly westward in the central Pacific; the migration of the front is related to the changes in strength of the zonal currents. In the frontal region, the zonal advection explains most of the SSS variability. The

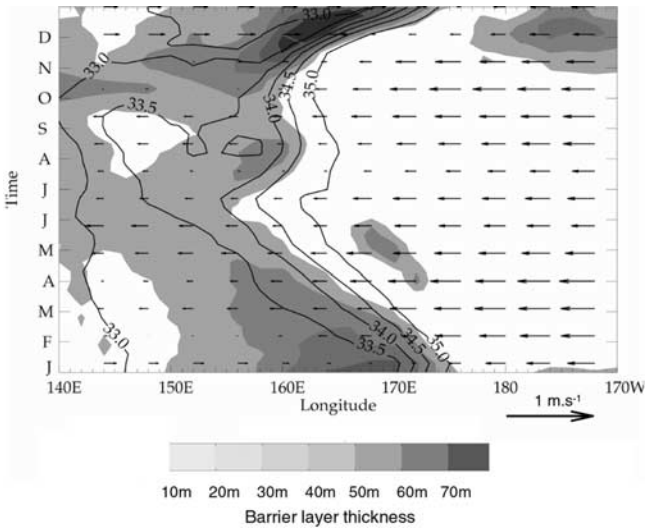

Figure 7. Longitude–time plot of SSS (contours), barrier layer thickness (gray tones) and surface zonal velocity (vectors) along the equator between 140°E and 170°W for the reference run.

salinity front is tighter, and the barrier layer is thicker when zonal velocity, induced by westerly wind, is clearly eastward in the warm pool. In this case, a strong downwelling is created by the zonal convergence near the salinity front, resulting in the subduction of the salty and dense water brought by the SEC under the fresh and light water of the warm pool, which is partly responsible for the deep thermocline near the eastern edge of the warm pool and, thus, of the barrier layer formation in the equatorial band [*Vialard and Delecluse*, 1998b]. This barrier layer is not a sporadic oceanic structure but a climatological feature of the Warm Pool [*Sprintall and Tomczack*, 1992]. The barrier layer is located in the fresh pool region west of the salinity front. Its thickness is related to the zonal gradient of SSS, thicker (thinner) when the front has sharpened (relaxed); *Delcroix and McPhaden* [2002] suggest using this SSS gradient as a proxy for barrier layer formation.

[40] The assimilation experiment begins on 1 January. This date corresponds to a time when the salinity front was located at its far eastern position (Figure 7). Zonal currents on the two sides of the front are of opposite sign, and a thick barrier layer is present west of the front. During the first 6 months of the year, the front migrates slowly westward under the effect of zonal advection. The initial condition chosen corresponds to a very different situation from the state of 1 January, as it is the model state at the middle of June. At this time, the salinity front is at its western most position, and it is relatively weak. Westward currents are dominant, and the barrier layer is thin. Figure 8 illustrates how the EFP is influenced by assimilation. Results are presented after a 1-month assimilation period. The free model still has the memory of the initial condition with a front located at 160°E, but eastward currents have been generated west of the front by the forcing which provide the condition for the front to move eastward (Figure 8a). Sea Surface Height (SSH) is high in the warm pool, and decreases to the east (Figure 8b), but the distinction between the warm/fresh pool and the water from the center of the basin is less clear in SSH than salinity. At this time, the assimilation results are very different from the free model with an eastward migration of the fresh pool corresponding to a front located at 170°E with a marked downwelling, and

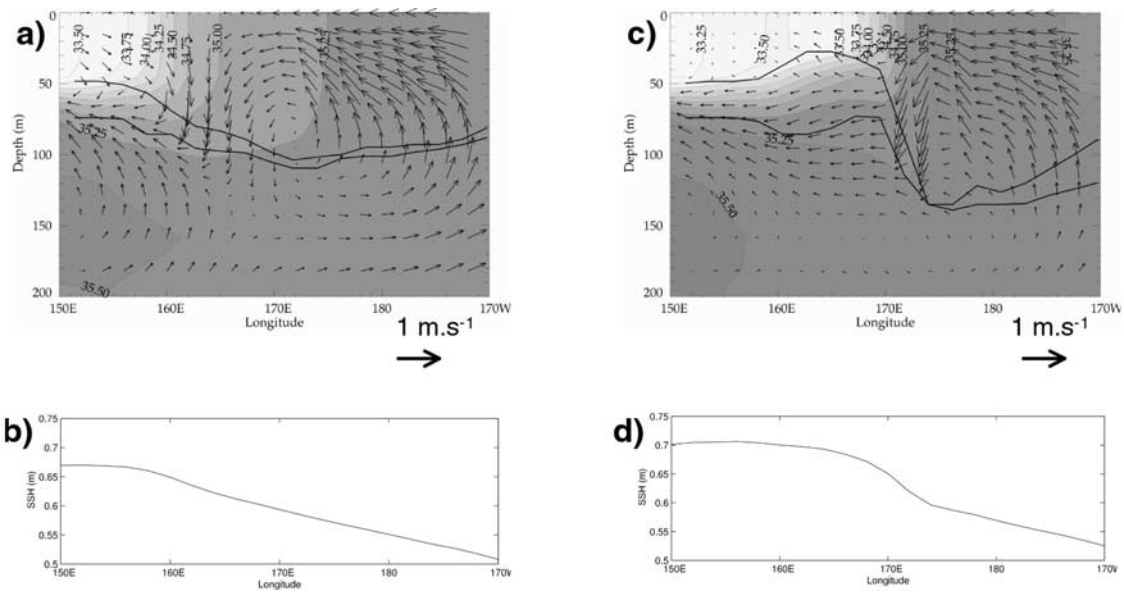

Figure 8. Longitude–depth section at the equator of salinity (contours) and velocity (vectors) for a) the model without assimilation and c) the model with assimilation. Iso-contours are every 0.25 psu. Superimposed in thick lines are the mixed layer depth (upper curve) and the isothermal layer depth (lower curve). The thickness between these two curves is representative of the barrier layer. b) Corresponding SSH signature for the model without assimilation and d) for the model with assimilation. All fields are snapshots after a one month long experiment (1 February).

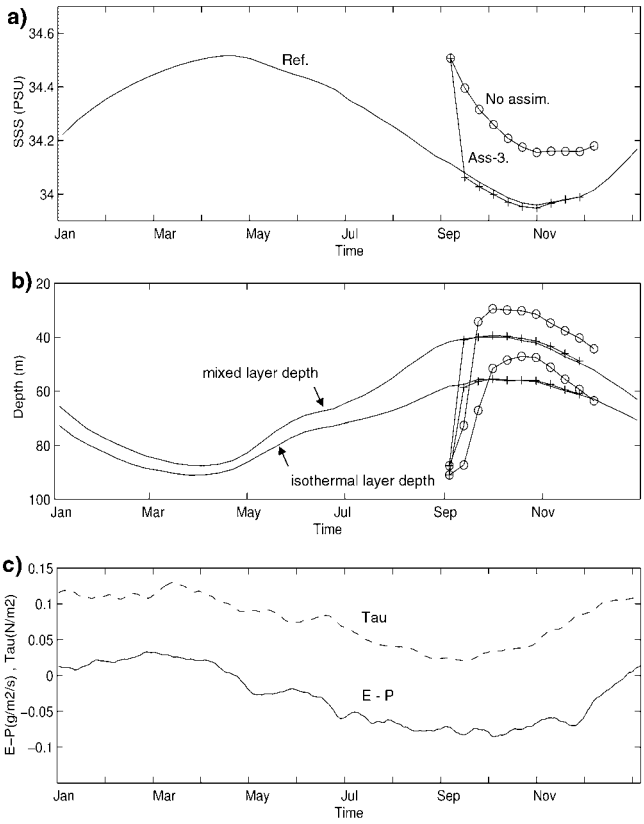

Figure 9. Assimilation working in the ITCZ. a) SSS evolution for the Reference, the model without (o) and with (+) assimilation. b) Time evolution of the mixed layer depth (upper curve) and isothermal layer depth (lower curve) for the reference (continuous line), the model without (o) and with (+) assimilation. The thickness between these two curves is representative of the barrier layer. c) Time evolution of the wind stress (dotted line), and Evaporation minus Precipitation (E-P, continuous line) forcing.

a thicker barrier layer 5–10 degrees to the West (Figure 8b). Differences in terms of SSH reach 7 cm. These results are very close to the reference (not shown, as it is similar to Figures 8c and 8d) although small differences exist; namely salinity is a little bit too salty in the fresh pool (i.e. 0.2 psu), the downwelling is a little bit stronger and a 2 cm SSH error is still present around the position of the front. (This error reflects a small difference in the location of the front, 2° too much in the west for the assimilation.) At this stage, it is interesting to note that even if our experiments are conducted with climatological forcing, the behavior of both the reference run and the assimilation run is largely consistent with the previous studies (for a perspective, compare our Figure 8c with Figure 7a in the work of *Vialard and Delecluse* [1998b]).

[41] As we saw in section 2, the ITCZ area corresponds to low salinity surface water, due to the strong freshwater flux from the atmosphere to the ocean there. The area of minimum SSS is situated 4°–6° north of the axis of maximum precipitation, a consequence of poleward Ekman transport associated with the trade winds [*Delcroix et al.*, 1996]. In terms of variability, the SSS seasonal cycle lags behind the E-P seasonal cycle (Figure 9). In other words, minimum (maximum) SSS occurs after minimum (maximum) E-P. The mean lag in the ITCZ box is 1–2 months, hence the two signals are not in exact quadrature. This can be explained by the fact that SSS variability is not exclusively driven by E-P variability. The North Equatorial Counter Current (NECC) has a marked seasonal cycle (not shown), and may also influence SSS variability via horizontal advection. The mixed layer depth variability seems to be driven by both the fresh water flux variability (which dominates buoyancy forcing in this region) and the dynamic forcing (wind induced turbulent vertical mixing) (Figure 9). The heavy rain/low wind periods are associated with mixed layer shoaling, above a deeper thermocline; hence a barrier layer is observed to develop during these periods. *Vialard and Delecluse* [1998b] suggest that the mechanism allowing the surface layer to maintain the same temperature as the underlying layer is similar to what occurs in the warm pool: the thin mixed layer transmits a significant fraction of the incident solar radiation across its base. In contrast, during low rain/high wind periods, the mixed layer deepens and attains almost the same depth as the thermocline and the barrier layer structure disappears.

[42] We take advantage of this contrast between high wind/low rain/deep mixed layer/thin barrier layer periods and low wind/strong rain/shallow mixed layer/thick barrier layer periods to build our assimilation experiment. It begins on 1 September. At this date, the ITCZ is at its northernmost position, and the NECC is fully developed (not shown). The mixed layer is relatively shallow with a 40 m depth, associated with low salinity surface water and a thick barrier layer (Figure 9). These conditions remain relatively stable during the following month. Our initial condition is chosen at the end of winter (1 April), and corresponds to the opposite situation. The ITCZ has migrated southward, and the NECC has disappeared. The mixed layer is thick (90 m depth), and there is almost no underlying barrier layer. The free model quickly reacts to the forcing with a shoaling in the mixed layer depth and the development of a barrier layer in less than 20 days (Figure 9). But the free model remains far from the reference with a too shallow mixed layer, a too high SSS, and subsurface thermal structure remaining near the initial condition (Figure 10). The SSS data assimilation efficiently constrain the mixed layer properties as soon as the first assimilation stage, and the subsequent assimilation trajectory remains close to the reference (Figure 9). The subsurface temperature structure and the associated geostrophic currents are also positively influenced by the assimilation (the differences between REF and MOD shown in Figure 9 have disappeared). This results in a meridional SSH structure with ridges and troughs similar to the reference (Figure 10).

[43] The hydrological characteristics of SPCZ area are quite similar to those of ITCZ area: it is a zone of low surface salinity water with a high SSS temporal variability (Figure 1). SSS variability lags behind E-P variability by about 3 months (Figure 11), which is consistent with SSS variations chiefly driven by the freshwater forcing flux. Like in the ITCZ area, the mixed layer depth exhibits a marked seasonal cycle; once again, this signal is consistent with the seasonal cycle of both buoyancy and momentum

forcing: during austral summer, precipitation is strong and wind stress is weak, which results in a shallow mixed layer over a thick barrier layer; during austral winter, freshwater supply is null, wind-induced turbulent mixing is strong and the resulting mixed layer is deep. However, there are some discrepancies between the behavior of the ITCZ and SPCZ areas. Indeed, it is not clear which processes allow the barrier layer to remain thick throughout austral winter, whereas freshwater supply is roughly null during this period (Figure 11). Moreover, explanation for the contrast between the slow thickening of the mixed layer from April to September and the rapid stratification of the upper ocean in October and November is not obvious. The effects of both the forcing at the surface and of the inner ocean dynamics might interact. The so-called Tropical Water characterized by a subsurface salinity maximum, which flows within the main thermocline, induces a marked vertical salinity gradient at the bottom of the mixed layer. This may interact with the mixed layer hydrological variability. Moreover, the area exhibits rather strong variability in upper layer horizontal currents, with the westward-flowing South Equatorial Current interrupted by the occasional eastward-flow of the South Equatorial Counter Current (during austral summer, not shown); this reversal might play a role in the upper layer thermohaline variability via horizontal advection.

[44] The assimilation experiment begins on 1 September, with an initial condition chosen on 1 April. Unlike the ITCZ area, it is interesting to notice that the free model tends to retain the initial condition in terms of mixed layer depth and isothermal layer depth (Figure 11). This could be explained by the fact that it is easier to transfer downward the constraint brought by the forcing fluxes in the case of a too deep initial mixed layer (like in the ITCZ area, at initial stage) than in the case of a too shallow layer (like in the SPCZ area, at initial stage). Indeed, the initial pycnocline being too shallow in the SPCZ area, it acts like a barrier to the downward penetration of the forcing fluxes and so the free model tends to retain a too shallow pycnocline depth. As for the assimilation, it behaves much like the ITCZ area: as soon as the first assimilation stage, the upper thermohaline structure is well corrected, leading to SSS, mixed layer depth and isothermal layer depth very close to the reference (Figure 11).

[45] On the whole, assimilation allows a proper simulation of the upper layer thermohaline structure, even if starting from an extreme initial condition that differs greatly from the mean field (the ideal initial condition for the SEEK performance from a theoretical viewpoint).

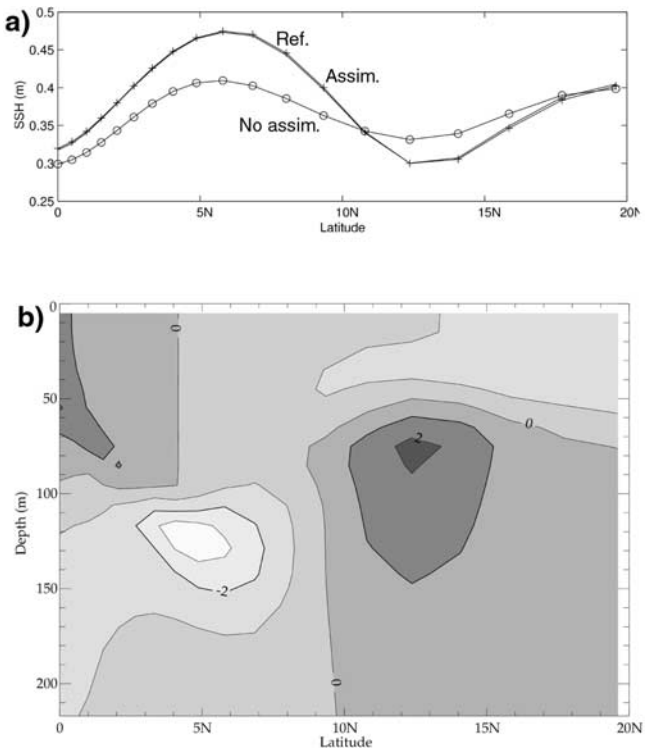

Figure 10. a) Meridional section of SSH along 165°E for the Reference (continuous line), the model without (o) and with (+) assimilation. b) Corresponding latitude–depth section of the difference of temperature between the model without assimilation and the Reference. All fields are snapshots after a one month long experiment (1 October).

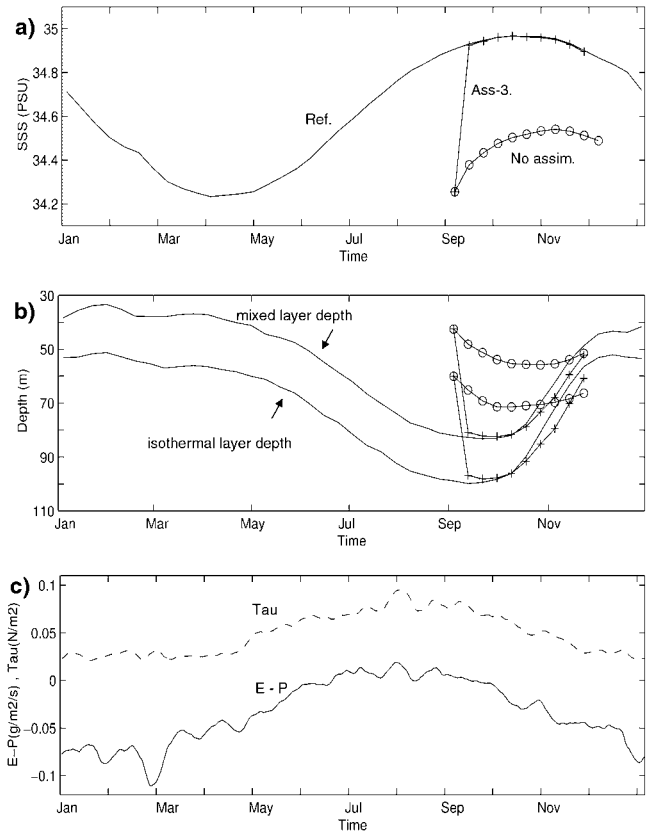

Figure 11. Same as Figure 9 for the SPCZ area.

6. Conclusion

[46] The objective of this paper is to assess the contribution of sea-surface salinity observations to the control of numerical simulations of the tropical Pacific Ocean. This work is motivated on the one hand by the recognition of the importance of salinity in the tropical Pacific Ocean in terms

of dynamics and thermodynamics and, on the other hand, by the prospect of the future satellite missions dedicated to SSS observations.

[47] The approach that has been taken here is based on the use of data assimilation: this technique is seen as a means (the only optimal means) to introduce in situ and remotely sensed salinity observations into a numerical model, and to make the numerical simulations closer to real ocean behavior. Data assimilation can also be seen as a tool to correct various model parameter inadequacies or for the optimal adjustment of certain model parameters and model forcing functions. In addition, data assimilation may be used to help optimize ocean observation systems. This is particularly true for satellite missions in order to determine critical accuracy criteria and adequate sampling strategy. In the present paper, the first point is the main issue under consideration (Can we control/improve ocean circulation with salinity data?), but the latter point (What is the appropriate strategy for a satellite mission?) is also constantly present in our mind.

[48] The ability of the SEEK filter to assimilate SSS data is clearly demonstrated by comparison with a conventional method of the Newtonian relaxation type. When tested in our model and even in the simple twin experiment situation, relaxation was found to be incapable of properly correcting the SSS field, and does not allow other variables, especially in-depth, to adjust for corrections provided by the SSS data. In contrast, the SEEK filter quasi-instantaneously allows control of the entire state vector. Again, this is done in the context of twin experiments in which the definition of error covariance is strictly in accordance with the system to be controlled. This is clearly a favorable case which will need further validation in a fully realistic situation. Implementation of the SEEK filter requires some truncating among the modes that are the most characteristic of the system's variability. A specific investigation has been conducted in this regard: the results were found to be rather sensitive to the truncating limit. To restrain the level of errors at a level of 0.1 psu Rms for surface salinity, the basis must represent at least 90% of the SSS variance.

[49] The assimilation of SSS data in simulating the case of a satellite mission based on the GODAE criteria shows that the data precision and sampling were found to produce little discrepancies in results. Measurement accuracy has been established at 0.2 psu Rms, assuming white noise distribution, and the SEEK filter was found quite adequate to filter this level of error properly. In addition, the model grid on which the data were defined, is fairly close to the GODAE specifications for data sampling ($2^\circ \times 2^\circ \times 10$ days). The inaccuracy resulting from this undersampling is small and is estimated at 0.06 psu rms. Depending on the variable, error is reduced to a level between 30% and 80% as early as the first analysis. As far as salinity is concerned, the best constraints are seen in the upper levels characteristic of the mixed layer, where salinity variability is the strongest. Regarding temperature and zonal velocity, surface fields and thermocline levels are better constrained than mixed layer levels. At a later stage, the errors decrease and stabilize at values that depend directly on the SSS residual error carried by the assimilation. The errors in salinity, temperature and zonal velocity are small: less than 0.04 psu, 0.15°C and 0.012 m/s respectively.

[50] Salinity can have a strong impact on the convergence zones and on the eastern edge of the fresh pool. SSS assimilation allows good control in these regions, particularly of SSH and zonal velocity in the fresh pool, which is a key factor for its displacement, and of the settings of barrier layers in the convergence areas. This demonstrates the promise of such a data assimilation approach for monitoring the ocean in these regions.

[51] These experiments have considerable limitations however, and are only a first step in studying the use of SSS data as may one-day be observed from satellite. More realistic situations must now be considered. The SSS signal assimilated here was fully coherent with the model dynamics/thermodynamics and with the forcing fields, which is not the case in reality. Further investigations must be undertaken where the SSS observations correspond to different forcing functions within the range of what can be expected in real situations. We have seen that the modeled SSS field is often biased with regard to observations. This question of bias must be considered per se and should probably not be resolved through standard data assimilation techniques where the hypothesis of "centered statistical variables" is ubiquitous. Some of these questions must be explored initially in the framework of twin experiments, before the actual use of satellite SSS data. A major issue should also be to consider the whole dimension of the ocean observing system, i.e. to take advantage of the complementary data-sets that are already available or that will become available during the future satellite missions. This concerns other satellite data but also in situ data, including data that will provide salinity measurements following a different measurement strategy (instrumental, sampling, accuracy, etc.) such as ARGO or the VOS networks.

[52] **Acknowledgments.** This work was partly supported by Noveltis and the Service Hydrographique et Océanographique de la Marine. We express our gratitude to Gurvan Madec and his team for having made available the ocean model. Technical support from Maurice Imbard was particularly appreciated. Jean-Michel Brankart, Laurent Parent and Charles-Emmanuel Testut have developed a powerful software that made the assimilation experiments and analysis so much easier. The plotting tools developed by Sebastien Masson were very helpful.

References

Acero-Schwertzer, C., D. Hansen, and M. Swenson, Evaluation and diagnosis of surface currents in the National Centers for Environmental Prediction's Ocean analyses, *J. Geophys. Res.*, *102*, 21,037–21,048, 1997.

Blanke, B., and P. Delecluse, Variability of the tropical Atlantic ocean simulated by a general circulation model with two different mixed layer physics, *J. Phys. Oceanogr.*, *23*, 1363–1388, 1993.

Cane, M., A. Kaplan, R. N. Miller, B. Tang, E. C. Hackert, and A. J. Busalacchi, Mapping tropical Pacific sea level: Data assimilation via a reduced state space Kalman filter, *J. Geophys. Res.*, *101*, 22,599–22,617, 1996.

Chen, D., M. A. Cane, S. E. Zebiak, and A. Kaplan, The impact of sea level data assimilation on the Lamont model prediction of the 1997/1998 El Niño, *Geophys. Res. Lett.*, *25*, 2837–2840, 1998.

Delcroix, T., Observed surface oceanic and atmospheric variability in the tropical pacific at seasonal and ENSO time scales: A tentative overview, *J. Geophys. Res.*, *103*, 18,611–18,633, 1998.

Delcroix, T., and G. Eldin, Observations Hydrologiques dans l'Océan Pacifique Tropical Ouest, Campagnes SURTROPAC 1 à 17, de janvier 1984 à août 1992, campagnes COARE156 1 à 3, d'août 1991 à octobre 1992. TDM 141, ORSTOM Editions, 78 pp., Paris, 1995.

Delcroix, T., and M. J. McPhaden, Interrannual sea surface salinity and temperature changes in the western Pacific warm pool during 1992–2000, *J. Geophys. Res.*, *107*, 10.1029/2001JC000862, in press, 2002.

Delcroix, T., and J. Picaut, Zonal displacement of the western equatorial Pacific fresh pool, *J. Geophys. Res.*, *103*, 1087–1098, 1998.

Delcroix, T., C. Hénin, V. Porte, and P. Arkin, Precipitation and sea surface salinity in the tropical Pacific Ocean, *Deep Sea Res., Part I*, *43*, 1123–1141, 1996.

Donguy, J. R., Surface and subsurface salinity in the tropical Pacific Ocean. Relations with climate, *Prog. Oceanogr.*, *34*, 45–78, 1994.

Eldin, G., M. Rodier, and M. H. Radenac, Physical and nutrient variability in the upper equatorial Pacific associated with westerly wind forcing and wave activity in October 1994, *Deep Sea Res.*, *44*, 1783–1800, 1997.

Fukumori, I., and P. Malanotte-Rizzoli, An approximate Kalman filter for ocean data assimilation: An example with an idealized Gulf Stream model, *J. Geophys. Res.*, *100*, 6777–6793, 1995.

Fukumori, I., R. Raghunath, L. L. Fu, and Y. Chao, Assimilation of TOPEX/Poseidon altimeter data into a global ocean circulation model: How good are the results?, *J. Geophys. Res.*, *104*, 25,647–25,665, 1999.

Gourdeau, L., J. Verron, T. Delcroix, A. J. Busalacchi, and R. Murtugudde, Assimilation of Topex/Poseidon altimetric data in a primitive equation model of the tropical Pacific ocean, during the 1992–1996 ENSO period, *J. Geophys. Res.*, *105*, 8473–8488, 2000.

Hénin, C., and J. Grelet, A merchant ship thermosalinograph network in the Pacific ocean, *Deep Sea Res., Part I*, *43*, 1833–1856, 1996.

Hénin, C., Y. du Penhoat, and M. Ioualalen, Observations of sea surface salinity in the western Pacific fresh pool: Large scale changes during 1992–1995, *J. Geophys. Res.*, *103*, 7523–7536, 1998.

Ji, M., R. W. Reynolds, and D. W. Behringer, Use of Topex/Poseidon sea level data for ocean analyses and ENSO prediction: Some early results, *J. Clim.*, *13*, 216–231, 2000.

Johnson, G. C., M. J. McPhaden, G. D. Rowe, and K. E. McTaggart, Upper equatorial Pacific ocean current and salinity variability during the 1996–1998 El Niño–La Niña cycle, *J. Geophys. Res.*, *105*, 1037–1053, 2000.

Kessler, W., Observations of long Rossby waves in the northern tropical Pacific, *J. Geophys. Res.*, *95*, 5183–5217, 1990.

Kuroda, Y., and M. J. McPhaden, Variability in the western equatorial pacific ocean during JAPACS cruises in 1989 and 1990, *J. Geophys. Res.*, *98*, 4747–4759, 1993.

Lagerloef, G., and T. Delcroix, Sea surface salinity: A regional case study for the tropical Pacific, in *Observing the Ocean in the 21st Century*, Australian Bureau of Meteorol., Melbourne, Australia, 2001.

Levitus, S., Annual cycle of salinity and salt storage in the world ocean, *J. Phys. Oceanogr.*, *16*, 322–343, 1986.

Levitus, S., T. P. Boyer, and J. Antonov, *World Ocean Atlas*, vol. 5, *Interannual Variability of Upper Ocean Thermal Structure*, NOAA Atlas NESDIS 5, 176 pp., U.S. Govt. Print. Off., Washington, D. C., 1994.

Lukas, R., The termination of the Equatorial Under Current in the eastern Pacific, *Progr. Oceanogr.*, *16*, 63–90, 1986.

Lukas, R., and E. Lindstrom, the mixed layer of the western equatorial Pacific ocean, *J. Geophys. Res.*, *96*, 3343–3357, 1991.

Madec, G., P. Delecluse, M. Imbard, and C. Levy, *OPA 8.1 Ocean General Circulation Model Reference Manual*, Note du Pole de modélisation, No. 11, 91 pp., Institut Pierre-Simon Laplace (IPSL), France, 1998.

McPhaden, M. J., et al., The Tropical Ocean–Global Atmosphere (TOGA) observing system: A decade of progress, *J. Geophys. Res.*, *103*, 14,169–14,240, 1998.

McPhaden, M., T. Delcroix, K. Hanawa, Y. Kuroda, G. Meyers, J. Picaut, and M. Swenson, The El Niño/Southern Oscillation (ENSO) observing system, in *Observing the Ocean in the 21st Century*, Australian Bureau of Meteorology, Melbourne, Australia, 2001.

Murtugudde, R., and A. J. Busalacchi, Salinity effects in a tropical ocean model, *J. Geophys. Res.*, *103*, 3283–3300, 1998.

Pham, D. T., J. Verron, and M. C. Roubaud, A singular evolutive extended Kalman filter for data assimilation in oceanography, *J. Mar. Syst.*, *16*, 323–340, 1998.

Picaut, J., and T. Delcroix, Equatorial wave sequence associated with the warm pool displacement during the 1986–1989 El Niño and La Niña, *J. Geophys. Res.*, *100*, 18,393–18,408, 1995.

Picaut, J., M. Ioualalen, C. Menkes, T. Delcroix, and M. J. McPhaden, Mechanism of the zonal displacements of the Pacific warm pool: Implications for ENSO, *Science*, *274*, 1486–1489, 1996.

Picaut, J., F. Masia, and Y. DuPenhoat, An advective–reflective conceptual model for the oscillatory nature of ENSO, *Science*, *277*, 663–666, 1997.

Picaut, J., M. Ioualalen, T. Delcroix, F. Masia, R. Murtugudde, and J. Vialard, Displacements of an oceanic zone of convergence on the eastern edge of the Pacific warm pool: Consequences for ENSO and biogeochemical phenomena, *J. Geophys. Res.*, *106*, 2363–2386, 2001.

Reynolds, R. W., M. Ji, and A. Leetmaa, Use of salinity to improve ocean modeling, *Phys. Chem. Earth*, *23*, 543–553, 1998.

Roemmich, D., et al., ARGO: The global array of profiling floats, in *Proceedings of the International Conference on the Ocean Observing System for Climate, 18–22 October, St. Raphael*, 1999.

Roullet, G., and G. Madec, Salt conservation, free-surface and varying levels: A new formulation for an Ocean GCM, *J. Geophys. Res.*, *105*, 23,927–23,942, 2000.

Segschneider, J., M. Balmaseda, and D. L. T. Anderson, Anomalous temperature and salinity variations in the tropical Atlantic: Possible causes and implication for the use of altimeter data, *Geophys. Res. Lett.*, *27*, 2281–2284, 2000.

Sprintall, J., and T. Tomczak, Evidence of the barrier layer in the surface layer of the tropics, *J. Geophys. Res.*, *97*, 7305–7316, 1992.

Verron, J., L. Gourdeau, D. T. Pham, R. Murtugudde, and A. J. Busalacchi, A singular evolutive extended Kalman filter to assimilate satellite altimeter data into a non-linear numerical model of the tropical Pacific: Method and validation, *J. Geophys. Res.*, *104*, 5441–5458, 1999.

Vialard, J., and P. Delecluse, An OGCM study for the TOGA decade, 1, Role of salinity in the physics of the western Pacific fresh pool, *J. Phys. Oceanogr.*, *28*, 1071–1088, 1998a.

Vialard, J., and P. Delecluse, An OGCM study for the TOGA decade, 2, Barrier layer formation and variability, *J. Phys. Oceanogr.*, *28*, 1089–1106, 1998b.

Vialard, J., P. Delecluse, and C. Menkes, A modelling study of salinity variability and effects in the tropical Pacific during the 1993–1999 period, *J. Geophys. Res*, *107*, 10.1029/2001JC000758, in press, 2002.

Vialard, J., C. Menkes, J. P. Boulanger, P. Delecluse, E. Guilyardi, M. J. McPhaden, and G. Madec, A model study of oceanic mechanisms affecting the equatorial Pacific sea surface temperature during the 1997–1998 El Nino, *J. Phys. Oceanogr.*, *31*, 1649–1675, 2001.

World Climate Research Program (WCRP), CLIVAR Initial Implementation Plan, WMO/TD-869, June 1998.

T. Delcroix, IRD, BPA5, Nouméa, 98848 New Caledonia, France.

F. Durand and L. Gourdeau, LEGOS, 14 Av. Edouard Belin, 31401 Toulouse, France. (Fabien.Durand@cnes.fr)

J. Verron, LEGI, UMR5519 CNRS, BP53X, 38041 Grenoble, France.